

# Generalized Multi-view Embedding for Visual Recognition and Cross-modal Retrieval

Guanqun Cao, Alexandros Iosifidis, *Senior Member, IEEE*, Ke Chen and Moncef Gabbouj, *Fellow, IEEE*

Dept. of Signal Processing, Tampere University of Technology, Finland

{guanqun.cao, alexandros.iosifidis, ke.chen, moncef.gabbouj}@tut.fi

**Abstract**—In this paper, the problem of multi-view embedding from different visual cues and modalities is considered. We propose a unified solution for subspace learning methods using the Rayleigh quotient, which is extensible for multiple views, supervised learning, and non-linear embeddings. Numerous methods including Canonical Correlation Analysis, Partial Least Square regression and Linear Discriminant Analysis are studied using specific intrinsic and penalty graphs within the same framework. Non-linear extensions based on kernels and (deep) neural networks are derived, achieving better performance than the linear ones. Moreover, a novel variant of multi-view Linear Discriminant Analysis is proposed by taking the view difference into consideration. We demonstrate the effectiveness of the proposed multi-view embedding methods on visual object recognition and cross-modal image retrieval, and obtain superior results in both applications compared to related methods.

## I. INTRODUCTION

People see the world differently, and objects are described from various point of views and modalities. Identifying an object can not only benefit from visual cues including color, texture and shape, but textual annotations from different observations and languages. Thanks to data enrichment from sensor technologies, the accuracy in image retrieval and recognition has been significantly improved by taking advantage of multi-view and cross-domain learning [1], [2]. Since matching the data samples across various feature spaces directly is infeasible, subspace learning approaches, which learn a common feature space from multi-view spaces, becomes an effective approach in solving the problem.

Numerous methods have been proposed in subspace learning. They can be grouped into three major categories based on the characteristics of machine learning: *two-view learning* and *multi-view learning*; *unsupervised learning* and *supervised learning*; and *linear learning* and *non-linear learning*. While traditional techniques in multivariate analysis take two inputs [3], multi-view methods have been proposed to find an optimal representation from more than two views [4], [5]. Compared to learning the feature transformation in an unsupervised manner, discriminative methods, such as Linear Discriminant Analysis (LDA) have been extended to multi-view cases. Additionally, the transformation can also be kernel-based or learned by (deep) neural nets to exploit their non-linear properties.

*Two-view learning* and *multi-view learning*: One of the most popular methods in multivariate statistics is Canonical Correlation Analysis (CCA) [6]. It seeks to maximize the correlation

between two sets of variables. Alternatively, its multi-view counterpart aims to obtain a common space from  $V > 2$  views [4], [5]. This is achieved by scaling the cross-covariance matrices to incorporate the covariances from more than two views. A similar approach to find the common subspace is Partial Least Square Regressions [7]. It maximizes the cross-covariance from two views by regressing the data samples to the common space. Besides transformation and regression, Multi-view Fisher Discriminant Analysis (MFDA) [8] learns the transformation minimizing the difference between data samples of predicted labels. A hierarchical clustering method was proposed to extend the limitation of binary classification in MFDA [9].

*Unsupervised learning* and *supervised learning*: In contrast to unsupervised transformations, including CCA and PLS, LDA [10] exploits the class labels effectively by maximizing the between-class scatter while minimizing the within-class scatter simultaneously. CCA has been successfully combined with LDA to find a discriminative subspace in [11], [12], [13]. Coupled Spectral Regression (CSR) [14] projects two different inputs to the low-dimensional embedding of labels by PLS regressions. Consistent with the original LDA, a Multi-view Discriminant Analysis (MvDA) [15] finds a discriminant representation over  $V$  views. The between-class scatter is maximized regardless of the difference between inter-view and intra-view covariances, while the within-class scatter is minimized in the mean time. Generalized Multi-view Analysis (GMA) [16] was proposed to maximize the intra-view discriminant information. It is an extension to CCA when class labels are available. Recently, a semi-supervised alternative [17] was also proposed for multi-view learning, which adopts a non-negative matrix factorization method for view mapping and a robust sparse regression model for clustering the labeled samples.

*Linear* and *non-linear learning*: Many problems are not linearly separable and thereby kernel-based methods and learning representation by (deep) neural nets are introduced. By mapping the features to the high dimensional feature space using the kernel trick [18], kernel CCA [19] adopts a pre-defined kernel and limits its application on small datasets. Many linear multi-view methods subsequently made their kernel extension [20], [13]. Kernel approximation [5] was adopted later to work on big data. Deep CCA [21] was proposed using neural nets to learn adaptive non-linear representations from two views, and uses the weights in the last layers to find the maximum correlation. A similar idea has been exploited on

LDA [22]. PCANet [23] was introduced to adopt a cascade of linear transformation, followed by binary hashing and block histograms.

Based on the aforementioned characteristics of subspace learning algorithms, we propose a generalized objective function for multi-view subspace learning using Rayleigh quotient. This unified multi-view embedding approach can be solved as a generalized eigenvalue problem. The intra-view and inter-view covariance matrices are scaled up to incorporate more than two views for CCA, PLS and LDA by exploiting their specific intrinsic and penalty graphs [10]. Moreover, we introduce novel multi-view LDA methods by using the distances between different class centers. We also extend the proposed method to the non-linear cases with kernels and (deep) neural networks. Kernel-based multi-view learning method is derived with an implicit kernel mapping. For larger datasets, we use the explicit kernel mapping [24] to approximate the kernel matrices. We also derive the formulation of stochastic gradient descent (SGD) for optimizing the objective function in the neural nets.

We demonstrate the effectiveness of the proposed embedding methods on visual object recognition and cross-modal image retrieval. Specifically, zero-shot recognition is evaluated by discovering novel object categories based on the underlying intermediate representation [25], [26], [27]. Its performance is heavily dependent on the representation in the latent space shared by visual and semantic cues. We integrate observations from *attributes* as a middle-level semantic property for the joint learning. Superior recognition results are achieved by exploiting the latent feature space with non-linear solutions learned from the multi-view representations. Cross-modal image retrieval is another multimedia application which interacts the visual content across modalities [1], [28], [29], [30]. In the experiments, we show promising retrieval results performed by embedding more modalities into the common feature space, and find that even conventional content-based image retrieval can be improved.

The rest of the paper is organized as follows. Section II reviews the related work. In Section III, we show the unified formulation to generalize the subspace learning methods. It is followed by the extension to multi-view techniques and derivation in kernels and neural nets. Then, in Section IV, we present the comparative results in zero-shot object recognition and cross-modal image retrieval on three popular multimedia datasets. Finally, Section V concludes the paper.

## II. RELATED WORK

In this section, we first define the common notations used throughout the paper. Then, we will briefly review the related methods for multi-view subspace learning. Moreover, recent work on non-linear methods concerning kernels and (deep) neural networks are discussed.

### A. Notations

We define the data matrix  $\mathbf{X} = [\mathbf{x}_1, \mathbf{x}_2, \dots, \mathbf{x}_N]$ ,  $\mathbf{x}_i \in \mathbb{R}^D$ , where  $N$  is the number of samples and  $D$  is the feature dimension. We also define  $\mathbf{X}_v \in \mathbb{R}^{D_v \times N}$ ,  $v = 1, \dots, V$  for



Fig. 1: Visualization of test images from the AwA dataset grouped by the features in the subspace. We bounded the leopard class in orange to show images of the same animal categories are positioned in their neighborhoods after multi-view embedding. Note the 2-dimensional t-SNE map [31] is generated from a near circular shape.

the feature vectors of the  $v$ th view, and discard the index in the single-view case for notation simplicity. Note that the dimensionality of the various feature spaces  $D_v$  may vary across the views. The covariance matrix is a statistics commonly used in CCA and PLS. We denote  $\bar{\mathbf{X}}_v = \mathbf{X}_v - \frac{1}{N} \mathbf{X}_v \mathbf{e} \mathbf{e}^\top$  as the centered data matrix. The covariance matrix is then expressed as

$$\Sigma_{ij} = \frac{1}{N} \bar{\mathbf{X}}_i \bar{\mathbf{X}}_j^\top = \frac{1}{N} \mathbf{X}_i \left( \mathbf{I} - \frac{1}{N} \mathbf{e} \mathbf{e}^\top \right) \mathbf{X}_j^\top, \quad (1)$$

where  $\mathbf{e} \in \mathbb{R}^N$  is a vector of ones and  $\mathbf{I} \in \mathbb{R}^{N \times N}$  is the identity matrix. For the supervised learning problems, the class label of the sample  $\mathbf{x}_i$  is noted as  $c_i \in \{1, 2, \dots, C\}$ , where  $C$  is the number of classes. We define the class vector  $\mathbf{e}^c \in \mathbb{R}^N$  with  $e_c(i) = 1$ , if  $c_i = c$ , and  $e_c(i) = 0$ , otherwise.  $\mathbf{W}_v \in \mathbb{R}^{D_v \times d}$ ,  $v = 1, \dots, V$  is the projection matrix for each view,  $d$  is the number of dimensions in the latent space and we discard the index in the single-view case. The feature dimension  $D_v$  in the original space of each view is usually high, which makes the distribution of the samples sparse, leading to several problems including the small sample size problem [32]. Therefore we want to project the samples to the latent space.

The generic projection function is defined to project  $\mathbf{X} \in \mathbb{R}^{D \times N}$  to  $\mathbf{Y} \in \mathbb{R}^{d \times N}$ . We define the linear projection by  $\mathbf{Y} = \mathbf{W}^\top \mathbf{X}$ . In kernel methods, we map the data to a Hilbert space  $\mathcal{F}$ . Let us define  $\phi(\cdot)$  as the non-linear function mapping  $x_i \in \mathbb{R}^D$  to  $\mathcal{F}$ , and  $\Phi = [\phi(\mathbf{x}_1), \dots, \phi(\mathbf{x}_N)]$  as the

data matrix in  $\mathcal{F}$ . In multi-view cases,  $\Phi = \begin{pmatrix} \Phi_1 \\ \vdots \\ \Phi_V \end{pmatrix}$ . Since the dimensionality of  $\mathcal{F}$  is arbitrary, the kernel trick [33] is exploited in order to implicitly map the data to  $\mathcal{F}$ . The Gram matrix is given by

$$\mathbf{K}_v = \kappa(\mathbf{X}_v, \mathbf{X}_v) = \Phi_v^\top \cdot \Phi_v, \quad (2)$$

where  $\kappa(\cdot, \cdot)$  is the so-called kernel function. The centered Gram matrix is

$$\bar{\mathbf{K}}_v = \mathbf{K}_v - \frac{1}{N} \mathbf{1} \mathbf{K}_v - \frac{1}{N} \mathbf{K}_v \mathbf{1}^\top + \frac{1}{N^2} \mathbf{1} \mathbf{K}_v \mathbf{1}. \quad (3)$$

In order to find the optimal projection, we can express  $\mathbf{W}_v$  of each view as a linear combination of the training samples in the kernel space based on the Representer Theorem [18], [34]. This can be expressed by using a new weight matrix  $\mathbf{A}_v$  as

$$\mathbf{W}_v = \Phi_v \mathbf{A}_v. \quad (4)$$

In the case where a neural network with  $M$  layers is considered,  $\beta_j$  contains the weight parameters in the  $j$ th layer,  $j = 1, \dots, M$ . The weights  $\mathbf{B} = [\beta_1, \dots, \beta_M]$  are learned by applying SGD, and  $h(\cdot; \mathbf{B})$  is a non-linear mapping function which maps  $\mathbf{X}_v$  to  $\mathbf{H}_v$ , i.e.

$$\mathbf{H}_v = h(\mathbf{X}_v; \mathbf{B}_v), \quad (5)$$

where  $\mathbf{B}_v$  is the weight matrix trained by applying backpropagation in the  $v$ th network.

### B. Canonical Correlation Analysis (CCA)

Canonical Correlation Analysis (CCA) [6], [35] is a conventional statistical technique which finds the maximum correlation between two sets of data samples  $\mathbf{X}_1 \in \mathbb{R}^{D_1 \times N}$  and  $\mathbf{X}_2 \in \mathbb{R}^{D_2 \times N}$  using the linear combination  $\mathbf{Y}_1 = \mathbf{W}_1^\top \mathbf{X}_1$  and  $\mathbf{Y}_2 = \mathbf{W}_2^\top \mathbf{X}_2$ .  $\mathbf{W}_1$  and  $\mathbf{W}_2$  are determined by optimizing:

$$\mathcal{J} = \arg \max_{\mathbf{W}_1, \mathbf{W}_2} \text{corr}(\mathbf{W}_1^\top \mathbf{X}_1, \mathbf{W}_2^\top \mathbf{X}_2) \quad (6)$$

$$= \arg \max_{\mathbf{W}_1, \mathbf{W}_2} \frac{\mathbf{W}_1^\top \Sigma_{12} \mathbf{W}_2}{\sqrt{\mathbf{W}_1^\top \Sigma_{11} \mathbf{W}_1} \cdot \sqrt{\mathbf{W}_2^\top \Sigma_{22} \mathbf{W}_2}}, \quad (7)$$

where

$$\Sigma = \begin{bmatrix} \Sigma_{11} & \Sigma_{12} \\ \Sigma_{21} & \Sigma_{22} \end{bmatrix} = \frac{1}{N} \begin{bmatrix} \bar{\mathbf{X}}_1 \bar{\mathbf{X}}_1^\top & \bar{\mathbf{X}}_1 \bar{\mathbf{X}}_2^\top \\ \bar{\mathbf{X}}_2 \bar{\mathbf{X}}_1^\top & \bar{\mathbf{X}}_2 \bar{\mathbf{X}}_2^\top \end{bmatrix} \quad (8)$$

### C. Kernel CCA

Kernel CCA finds the maximum correlation between two views after mapping them to the kernel space [19]. This is expressed by

$$\mathcal{J} = \arg \max_{\mathbf{W}_1, \mathbf{W}_2} \text{corr}(\mathbf{W}_1^\top \Phi_1, \mathbf{W}_2^\top \Phi_2) \quad (9)$$

We use the kernel trick in (4) and the Representer Theorem, and derive the objective function for the kernel CCA as

$$\mathcal{J} = \arg \max_{\mathbf{A}_1, \mathbf{A}_2} \frac{\mathbf{A}_1^\top \mathbf{K}_1 \mathbf{K}_2 \mathbf{A}_2}{\sqrt{\mathbf{A}_1^\top \mathbf{K}_1 \mathbf{K}_1 \mathbf{A}_1} \cdot \sqrt{\mathbf{A}_2^\top \mathbf{K}_2 \mathbf{K}_2 \mathbf{A}_2}}. \quad (10)$$

### D. Deep CCA

Deep CCA maximizes the correlation between a pair of views by learning non-linear representations from the input data through multiple stacked layers of neurons [21], [36]. A linear CCA layer is added to on top of both networks, and the inputs to the CCA layer depend on the network outputs  $\mathbf{H}_1$  and  $\mathbf{H}_2$ . Similar to the non-linear case in (10), a modified objective function is optimized

$$\min_{\mathbf{W}_1, \mathbf{W}_2} -\frac{1}{N} \text{Tr}(\mathbf{W}_1^\top \mathbf{H}_1 \mathbf{H}_2 \mathbf{W}_2), \quad (11)$$

where  $\mathbf{W}_1, \mathbf{W}_2$  are the projection matrices in the CCA layer, and the correlated outputs are  $\mathbf{Y}_1 = \mathbf{W}_1^\top \mathbf{H}_1$  and  $\mathbf{Y}_2 = \mathbf{W}_2^\top \mathbf{H}_2$ . A modified SGD method is developed with respect to the inputs  $\mathbf{H}_1$  and  $\mathbf{H}_2$  to the linear layer, which are also the outputs from the two networks. The objective function is expressed as  $\text{Tr}(\mathbf{W}_1^\top \mathbf{H}_1 \mathbf{H}_2 \mathbf{W}_2) = \text{Tr}(\mathbf{T}^\top \mathbf{T})^{\frac{1}{2}}$ , which describes the correlation as the sum of the top  $d$  singular vectors of  $\mathbf{T} = \Sigma_{11}^{-1/2} \Sigma_{12} \Sigma_{22}^{-1/2}$  whose definition can be found in [3].

### E. Partial Least Squares (PLS) regression

Partial Least Squares (PLS) regression [7] is another dimension reduction technique derived from the linear combination of the input vectors  $\mathbf{X}_1$  together with the target information which is considered as the second view  $\mathbf{X}_2$ . PLS maximizes the between-view covariance by solving

$$\mathcal{J} = \arg \max_{\mathbf{W}_1, \mathbf{W}_2} [\text{Tr}(\mathbf{W}_1^\top \mathbf{X}_1 \mathbf{X}_2^\top \mathbf{W}_2)], \quad (12)$$

$$\text{subject to } \mathbf{W}_1^\top \mathbf{W}_1 = \mathbf{I}, \mathbf{W}_2^\top \mathbf{W}_2 = \mathbf{I}. \quad (13)$$

The non-linear extensions of PLS are obtained in the similar manner as the ones in CCA.

### F. Linear Discriminant Analysis (LDA)

Linear Discriminant Analysis (LDA) [10], [37] finds the projection by maximizing the ratio of the between-class scatter to the within-class scatter. Let us define by  $\mu_c$  the mean vector of the  $c$ 'th class, formed by  $N_c$  samples, and  $\mu$  the global mean. Then, LDA optimizes the following criterion:

$$\mathcal{J} = \arg \max_{\mathbf{W}} \frac{\text{Tr}(\mathbf{W}^\top \mathbf{P} \mathbf{W})}{\text{Tr}(\mathbf{W}^\top \mathbf{Q} \mathbf{W})}, \quad (14)$$

where

$$\mathbf{P} = \sum_{c=1}^C N_c (\mu_c - \mu)(\mu_c - \mu)^\top = \mathbf{X} \left( \sum_{c=1}^C \frac{1}{N_c} \mathbf{e}_c \mathbf{e}_c^\top - \frac{1}{N} \mathbf{e} \mathbf{e}^\top \right) \mathbf{X}^\top, \quad (15)$$

$$\mathbf{Q} = \sum_{i=1}^N (\mathbf{x}_i - \mu_c)(\mathbf{x}_i - \mu_c)^\top = \mathbf{X} \left( \mathbf{I} - \sum_{c=1}^C \frac{1}{N_c} \mathbf{e}_c \mathbf{e}_c^\top \right) \mathbf{X}^\top. \quad (16)$$

### G. Multi-view Discriminant Analysis (MvDA)

A direct extension of LDA to multi-view cases was proposed in [15], [38]. In MvDA, the between-class variance is maximized regardless of view differences, while the within-class variance are minimized. The objective function is

$$\begin{aligned} \mathcal{J} &= \arg \max_{\mathbf{W}} \frac{\text{Tr}(\mathbf{W}^\top \mathbf{P} \mathbf{W})}{\text{Tr}(\mathbf{W}^\top \mathbf{Q} \mathbf{W})} \\ &= \arg \max_{\mathbf{W}} \frac{\text{Tr}(\sum_{c=1}^C N_c \mathbf{W}^\top (\boldsymbol{\mu}_c - \boldsymbol{\mu})(\boldsymbol{\mu}_c - \boldsymbol{\mu})^\top \mathbf{W})}{\text{Tr}(\sum_{c=1}^C \sum_{v=1}^V \sum_{i=1}^{N_{cv}} \mathbf{W}^\top (\mathbf{x}_i - \boldsymbol{\mu}_c)(\mathbf{x}_i - \boldsymbol{\mu}_c)^\top \mathbf{W})}. \end{aligned} \quad (17)$$

$$(18)$$

$\mathbf{P}_{jk}$  and  $\mathbf{Q}_{jk}$ , which are block submatrices of  $\mathbf{P}$  and  $\mathbf{Q}$  where  $j, k = 1, \dots, V$ , are defined as

$$\mathbf{P}_{jk} = \sum_{c=1}^C -\frac{N_{cj}N_{ck}}{N_c} \boldsymbol{\mu}_{cj} \boldsymbol{\mu}_{ck}^\top - \frac{1}{N} \left( \sum_{c=1}^C N_{cj} \boldsymbol{\mu}_{cj} \right) \left( \sum_{c=1}^C N_{ck} \boldsymbol{\mu}_{ck} \right)^\top,$$

and

$$\mathbf{Q}_{jk} = \begin{cases} \sum_{c=1}^C \left( \sum_{i=1}^{N_{cj}} \mathbf{x}_i \mathbf{x}_i^\top - \frac{N_{cj}^2}{N_c} \boldsymbol{\mu}_{cj} \boldsymbol{\mu}_{cj}^\top \right), & \text{if } j = k \\ \sum_{c=1}^C -\frac{N_{cj}N_{ck}}{N_i} \boldsymbol{\mu}_{cj} \boldsymbol{\mu}_{ck}^\top, & \text{otherwise.} \end{cases}$$

Here  $\boldsymbol{\mu}_{cj}$  denotes the mean of the  $c$ th class in the  $j$ th view.  $N_{cj}$  and  $N_c$  are the number of samples from the  $j$ th view of the  $c$ th class and total samples from the  $c$ th class, respectively.

### III. GENERALIZED MULTI-VIEW EMBEDDING

Here we propose a generalized expression of objective function for multi-view subspace learning. The generalized optimization problem is given by:

$$\mathcal{J} = \arg \max_{\mathbf{W}} \frac{\text{Tr}(\mathbf{W}^\top \mathbf{P} \mathbf{W})}{\text{Tr}(\mathbf{W}^\top \mathbf{Q} \mathbf{W})} \quad (19)$$

where  $\mathbf{P}$  and  $\mathbf{Q}$  are the matrices describing the inter-view and intra-view covariances, respectively. The above equation has the form of the Rayleigh quotient. Therefore, all subspace learning methods that maximize the criterion can be reduced to a generalized eigenvalue problem:

$$\mathbf{P} \mathbf{W} = \rho \mathbf{Q} \mathbf{W}, \quad (20)$$

and the solution is given in (21) below:

$$\mathbf{W} = \begin{pmatrix} \mathbf{W}_1 \\ \vdots \\ \mathbf{W}_V \end{pmatrix} \text{ and } \rho = \sum_{i=1}^d \lambda_i \quad (21)$$

are the generalized eigenvector and the sum of the top  $d$  generalized eigenvalues  $\lambda_i$  respectively.  $\mathbf{W}$  contains the projection matrices of all views, and  $\rho$  is the value of Rayleigh quotient. We take the top  $d$  dimensions of eigenvectors into the projection matrix, and their corresponding eigenvalues for  $\rho$  as the solution. We address the Rayleigh quotient as the uniform objective function, reaching out to all subspace learning methods in the paper. The non-linear multi-view embeddings can be achieved by kernel mappings, or (deep) neural networks optimized by SGD. Suppose we have a linear projection  $\mathbf{Y} = \mathbf{W}^\top \mathbf{X}$ ,  $\mathbf{S}_{vij}$  is a similarity weight matrix which encodes the intra-view properties to be minimized, and  $\mathbf{S}'_{vij}$  is a penalty weight expressing the inter-view properties to be maximized. Then based on [10], [39], we can express

the objective function as follows

$$\begin{aligned} \mathcal{J} &= \arg \max_{\mathbf{W}^\top \mathbf{W} = \mathbf{I}} \frac{\sum_{v=0}^V \sum_{i=0}^N \sum_{j=0}^N \mathbf{S}'_{vij} \|\mathbf{W}_v^\top \mathbf{X}_{vi} - \mathbf{W}_v^\top \mathbf{X}_{vj}\|^2}{\sum_{v=0}^V \sum_{i=0}^N \sum_{j=0}^N \mathbf{S}_{vij} \|\mathbf{W}_v^\top \mathbf{X}_{vi} - \mathbf{W}_v^\top \mathbf{X}_{vj}\|^2} \\ &= \arg \max_{\mathbf{W}^\top \mathbf{W} = \mathbf{I}} \frac{\text{Tr}(\mathbf{W}^\top \mathbf{X} \mathbf{L}' \mathbf{X}^\top \mathbf{W})}{\text{Tr}(\mathbf{W}^\top \mathbf{X} \mathbf{L} \mathbf{X}^\top \mathbf{W})}. \end{aligned} \quad (22)$$

$$(23)$$

In the kernel case, we also have

$$\mathcal{J} = \arg \max_{\mathbf{A}^\top \mathbf{K} \mathbf{A} = \mathbf{I}} \frac{\text{Tr}(\mathbf{A}^\top \mathbf{K} \mathbf{L}' \mathbf{K} \mathbf{A})}{\text{Tr}(\mathbf{A}^\top \mathbf{K} \mathbf{L} \mathbf{K} \mathbf{A})}. \quad (24)$$

In the above, we define the diagonal matrix of each view pair as  $\mathbf{D}_{uv}$  whose  $i$ -th element is  $[\mathbf{D}_{uv}]_{ii} = \sum_j [\mathbf{S}_{uv}]_{ij}$ , and the total graph Laplacian matrix as  $\mathbf{L} = \mathbf{D} - \mathbf{S}$ . Similarly, we have  $\mathbf{D}'$ ,  $\mathbf{S}'$ ,  $\mathbf{L}'$  in the penalty graph.

For the non-linear mapping by neural networks, we deploy a linear embedding layer on top of the networks. This scheme is illustrated in Fig. 2. Since we have more than two input views, we train multiple neural networks whose outputs are connected to the linear layer and the objective is the same as in the linear case. Through backpropagation, we optimize the Rayleigh quotient criterion with respect to all trained inputs to the last layer. The projection is found in the same way as in the linear case, and we will address the SGD formulation for the specific algorithms in the next section.

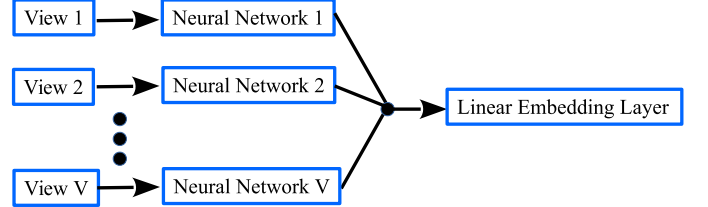


Fig. 2: An illustration of Multi-view (Deep) Embedding Networks.

Fig. 3 illustrates the proposed framework graphically. We can extract different types of low-level features from images, texts, and intermediate representations. The multi-modal feature vectors are passed through linear or non-linear projections to the latent space. The projected features characterize the properties of the inter-view separability and intra-view compactness based on the proposed criterion. We show the scaled inter-view and intra-view matrices for each multi-view algorithm in the next section. Then, the projection matrices are presented with respect to their own intrinsic and penalty graph matrices and the optimization methods.

#### A. Scaling up the inter-view and intra-view covariance matrices

The idea behind multi-view CCA is to maximize the correlation between all pairs of views. Its objective can be rephrased as maximizing the inter-view covariance while minimizing the intra-view covariance in the latent space. Therefore, we consider inter-view covariance matrices between different view representations in  $\mathbf{P}$  and the covariance matrices of each view in  $\mathbf{Q}$ . Multi-view PLS maximizes the intra-view covariance

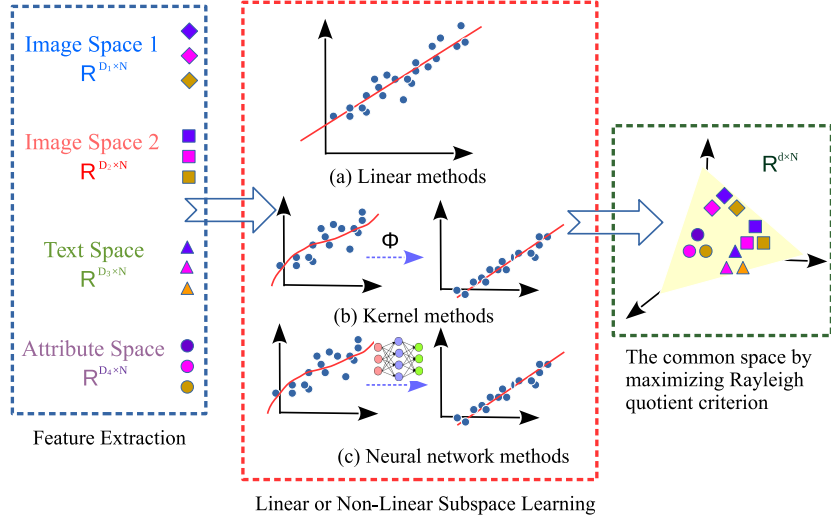


Fig. 3: Overview of multi-view embedding: Features from different modalities are extracted and mapped into the common subspace by maximizing the Rayleigh quotient criterion.

directly. Since we also embed the target information for the subspace learning, PLS differs from CCA only in the intra-view minimization. Taking the class discrimination into consideration, the novel multi-view LDA extends to separate the data of different classes between views while making the intra-class data compact. We illustrate  $\mathbf{P}$  and  $\mathbf{Q}$  for each method in Table I.

TABLE I: The matrices  $\mathbf{P}$  and  $\mathbf{Q}$  for the proposed multi-view CCA, PLS and LDA.

	$\mathbf{P}$	$\mathbf{Q}$
CCA	$\begin{bmatrix} \mathbf{0} & \Sigma_{12} & \cdots & \Sigma_{1V} \\ \Sigma_{21} & \mathbf{0} & \cdots & \Sigma_{2V} \\ \vdots & \vdots & \ddots & \vdots \\ \Sigma_{V1} & \Sigma_{V2} & \cdots & \mathbf{0} \end{bmatrix}$	$\begin{bmatrix} \Sigma_{11} & \mathbf{0} & \cdots & \mathbf{0} \\ \mathbf{0} & \Sigma_{22} & \cdots & \mathbf{0} \\ \vdots & \vdots & \ddots & \vdots \\ \mathbf{0} & \mathbf{0} & \cdots & \Sigma_{VV} \end{bmatrix}$
PLS	$\begin{bmatrix} \mathbf{0} & \Sigma_{12} & \cdots & \Sigma_{1V} \\ \Sigma_{21} & \mathbf{0} & \cdots & \Sigma_{2V} \\ \vdots & \vdots & \ddots & \vdots \\ \Sigma_{V1} & \Sigma_{V2} & \cdots & \mathbf{0} \end{bmatrix}$	$\begin{bmatrix} \mathbf{I} & \mathbf{0} & \cdots & \mathbf{0} \\ \mathbf{0} & \mathbf{I} & \cdots & \mathbf{0} \\ \vdots & \vdots & \ddots & \vdots \\ \mathbf{0} & \mathbf{0} & \cdots & \mathbf{I} \end{bmatrix}$
LDA	$\begin{bmatrix} \mathbf{P}_{11} & \mathbf{P}_{12} & \cdots & \mathbf{P}_{1V} \\ \mathbf{P}_{21} & \mathbf{P}_{22} & \cdots & \mathbf{P}_{2V} \\ \vdots & \vdots & \ddots & \vdots \\ \mathbf{P}_{V1} & \mathbf{P}_{V2} & \cdots & \mathbf{P}_{VV} \end{bmatrix}$	$\begin{bmatrix} \mathbf{Q}_{11} & \mathbf{0} & \cdots & \mathbf{0} \\ \mathbf{0} & \mathbf{Q}_{22} & \cdots & \mathbf{0} \\ \vdots & \vdots & \ddots & \vdots \\ \mathbf{0} & \mathbf{0} & \cdots & \mathbf{Q}_{VV} \end{bmatrix}$

### B. Linear subspace learning

When the subspace projection is linear, we can obtain the latent feature vectors from each view as

$$\mathbf{Y}_v = \mathbf{W}_v^\top \mathbf{X}_v, \quad (25)$$

and the projection matrix is derived directly by solving the generalized eigenvalue problem in (20). As shown in Table I, multi-view CCA has the total covariance matrix  $\Sigma = \mathbf{P} + \mathbf{Q}$ ,

and we derive its projection matrix by fulfilling the criterion below

$$\mathcal{J} = \arg \max_{\mathbf{w}_v, v=1, \dots, V} \frac{\text{Tr} \left( \sum_{i=1}^V \sum_{\substack{j=1 \\ j \neq i}}^V \mathbf{W}_i^\top \mathbf{X}_i \mathbf{L} \mathbf{X}_j^\top \mathbf{W}_j \right)}{\text{Tr} \left( \sum_{i=1}^V \mathbf{W}_i^\top \mathbf{X}_i \mathbf{L} \mathbf{X}_i^\top \mathbf{W}_i \right)}, \quad (26)$$

where the Laplacian matrix  $\mathbf{L} = \mathbf{I} - \frac{1}{N} \mathbf{e} \mathbf{e}^\top$ .

Multi-view PLS has the same Laplacian matrix as the one in Multi-view CCA. We only optimize the Rayleigh quotient by maximizing the cross-covariance matrices between different views as

$$\mathcal{J} = \arg \max_{\mathbf{W}^\top \mathbf{W} = \mathbf{I}} \text{Tr} \left( \sum_{i=1}^V \sum_{\substack{j=1 \\ j \neq i}}^V \mathbf{W}_i^\top \mathbf{X}_i \mathbf{L} \mathbf{X}_j \mathbf{W}_j \right), \quad (27)$$

whose solution is the projection matrix.

We propose two ways to determine the projection matrix in multi-view LDA. The first approach is the straightforward multi-view extension of the standard LDA, and its between-class scatter  $\mathbf{S}_B$  maximizes the distance between the class means regardless of their view origins:

$$\begin{aligned} \mathbf{S}_B &= \sum_{i=1}^V \sum_{j=1}^V \sum_{\substack{p=1 \\ p \neq q}}^C \sum_{q=1}^C (m_p^i - m_q^j)(m_p^i - m_q^j)^\top \\ &= \sum_{i=1}^V \sum_{j=1}^V \sum_{p=1}^C \sum_{q=1}^C \mathbf{W}_i^\top \mathbf{P}_{ij} \mathbf{W}_j, \end{aligned} \quad (28)$$

where  $\mathbf{P}_{ij} = \mathbf{X}_i \mathbf{L}_B \mathbf{X}_j^\top$ , and the between-class Laplacian matrix is

$$\mathbf{L}_B = \begin{cases} 2V \mathbf{e}_p \mathbf{e}_p^\top - 2 \mathbf{e}_p \mathbf{e}_q^\top & \text{if } i = j, \\ -2 \mathbf{e}_p \mathbf{e}_q^\top & \text{if } i \neq j. \end{cases} \quad (29)$$

$m_p^i$  denotes the mean from the  $i$ th view of the  $p$ th class in the latent space, and  $\mathbf{e}_p$  and  $\mathbf{e}_q$  are the  $N$ -dimensional class vector.

Alternatively, we propose the between-class scatter matrix which maximizes the distance between different class centers of different views as

$$\begin{aligned} \mathbf{S}'_B &= \sum_{i=1}^V \sum_{j=1}^V \sum_{p=1}^C \sum_{\substack{q=1 \\ p \neq q}}^C (\mathbf{m}_p^i - \mathbf{m}_q^i)(\mathbf{m}_p^j - \mathbf{m}_q^j)^\top \\ &= \sum_{i=1}^V \sum_{j=1}^V \sum_{p=1}^C \sum_{q=1}^C \mathbf{W}_i^\top \mathbf{X}_i \mathbf{L}'_B \mathbf{X}_j^\top \mathbf{W}_j, \end{aligned} \quad (30)$$

and the Laplacian matrix is

$$\mathbf{L}'_B = 2(\mathbf{e}_p \mathbf{e}_p^\top - \mathbf{e}_p \mathbf{e}_q^\top). \quad (31)$$

The difference between the two approaches is in that  $\mathbf{S}_B$  has  $(V-1) \sum_{i=1}^V \sum_{c=1}^C \mathbf{W}_i^\top \mathbf{X}_i \mathbf{e}_c \mathbf{e}_c^\top \mathbf{X}_i^\top \mathbf{W}_i / N_c^2$ , while  $\mathbf{S}'_B$  has the term  $\sum_{i=1}^V \sum_{j=1}^V \sum_{c=1}^C \mathbf{W}_i^\top \mathbf{X}_i \mathbf{e}_c \mathbf{e}_c^\top \mathbf{X}_j^\top \mathbf{W}_j / N_c^2$  which suggests that the first proposal only considers the maximum of the intra-view distances, while the second proposal can maximize the distance between different views. We also validate experimentally that the second proposal achieves better results. Detailed derivation of the two approaches of (28) and (30) are included in Appendix A.

We extend the same formulation of within-class Laplacian matrix in the latent space as the single-view LDA, i.e.

$$\begin{aligned} \mathbf{S}_W &= \sum_{i=1}^V \sum_{c=1}^C \mathbf{W}_i^\top \mathbf{X}_i \left( \mathbf{I} - \sum_{c=1}^C \frac{1}{N_c} \mathbf{e}_c \mathbf{e}_c^\top \right) \mathbf{X}_i^\top \mathbf{W}_i \\ &= \sum_{i=1}^V \sum_{i=1}^V \sum_{c=1}^C \mathbf{W}_i^\top \mathbf{Q}_{ii} \mathbf{W}_i, \end{aligned} \quad (32)$$

where  $\mathbf{Q}_{ii} = \mathbf{X}_i \mathbf{L}_W \mathbf{X}_i^\top$ , and  $\mathbf{L}_W = \mathbf{I} - \sum_{c=1}^C \frac{1}{N_c} \mathbf{e}_c \mathbf{e}_c^\top$ . From (28) and (32), it is shown that the between-class and within-class scatters are equivalent to the projected inter-view and intra-view covariance, respectively. The projection matrix of the multi-view LDA is found by optimizing the following objective function

$$\mathcal{J} = \arg \max_{\mathbf{W}_v, v=1, \dots, V} \frac{\text{Tr} \left( \sum_{i=1}^V \sum_{j=1}^V \sum_{p=1}^C \sum_{q=1}^C \mathbf{W}_i^\top \mathbf{X}_i \mathbf{L}_B^* \mathbf{X}_j^\top \mathbf{W}_j \right)}{\text{Tr} \left( \sum_{i=1}^V \sum_{c=1}^C \mathbf{W}_i^\top \mathbf{X}_i \mathbf{L}_W \mathbf{X}_i^\top \mathbf{W}_i \right)}, \quad (33)$$

where  $\mathbf{L}_B^*$  is denoted as the Laplacian matrix of either  $\mathbf{L}_B$  or  $\mathbf{L}'_B$ .

### C. Kernel-based non-linear subspace learning

Exploiting the kernel trick in (2) and the Representer theorem in (4), (25) can be expressed as follows

$$\mathbf{Y}_v = \mathbf{A}_v^\top \Phi_v^\top \Phi_v = \mathbf{A}_v^\top \mathbf{K}_v. \quad (34)$$

The criterion of kernel multi-view CCA is then,

$$\mathcal{J} = \arg \max_{\mathbf{K}_v, v=1, \dots, V} \frac{\text{Tr} \left( \sum_{i=1}^V \sum_{\substack{j=1 \\ j \neq i}}^V \mathbf{A}_i^\top \mathbf{K}_i \mathbf{L} \mathbf{K}_j \mathbf{A}_j \right)}{\text{Tr} \left( \sum_{i=1}^V \mathbf{A}_i^\top \mathbf{K}_i \mathbf{L} \mathbf{K}_i \mathbf{A}_i \right)}. \quad (35)$$

It can be easily shown that the solution for  $\mathbf{A}_v$  is the same as (20).

Kernel multi-view PLS maximizes the covariance between pairs of feature vectors in the kernel space and therefore the objective function is

$$\mathcal{J} = \arg \max_{\mathbf{K}_v, v=1, \dots, V} \text{Tr} \left( \sum_{i=1}^V \sum_{\substack{j=1 \\ j \neq i}}^V \mathbf{A}_i^\top \mathbf{K}_i \mathbf{L} \mathbf{K}_j \mathbf{A}_j \right). \quad (36)$$

The criterion for kernel multi-view LDA is

$$\mathcal{J} = \arg \max_{\mathbf{K}_v, v=1, \dots, V} \frac{\text{Tr} \left( \sum_{i=1}^V \sum_{j=1}^V \sum_{p=1}^C \sum_{q=1}^C \mathbf{A}_i^\top \mathbf{K}_i \mathbf{L}_B^* \mathbf{K}_j^\top \mathbf{A}_j \right)}{\text{Tr} \left( \sum_{i=1}^V \sum_{c=1}^C \mathbf{A}_i^\top \mathbf{K}_i \mathbf{L}_W \mathbf{K}_i^\top \mathbf{A}_i \right)}. \quad (37)$$

### D. Non-linear subspace learning using neural networks

Exploiting the non-linear mapping using neural networks by (5), (25) can be expressed as

$$\mathbf{Y}_v = \mathbf{W}_v^\top h(\mathbf{X}_v; \mathbf{B}_v) = \mathbf{W}_v^\top \mathbf{H}_v. \quad (38)$$

Since the network outputs are combined by a linear layer as shown in Fig. 2, the parameters  $\mathbf{B}_v$  of each network are jointly trained to reach the optimal criterion value. After the transformation by neural networks, the projection becomes the same as the multi-view linear subspace learning with respect to  $\mathbf{H}_v$ . Therefore, we need an additional optimization solved by SGD. We experimented with SGD without variance constraints, and found that we could obtain a much better result with the projections constrained to have the unit variance, i.e. in multi-view CCA, we have

$$\sum_{i=1}^V \mathbf{W}_i^\top \mathbf{H}_i \mathbf{L} \mathbf{H}_i \mathbf{W}_i = \mathbf{I}. \quad (39)$$

Without intra-view minimization, multi-view PLS optimization is constrained to have unit variance  $\sum_{i=1}^V \mathbf{W}_i^\top \mathbf{W}_i = \mathbf{I}$ , while in multi-view LDA, we project the between-class scatter into unit, i.e.

$$\sum_{i=1}^V \mathbf{W}_i^\top \mathbf{H}_i \mathbf{L}_W \mathbf{H}_i^\top \mathbf{W}_i = \mathbf{I} \quad (40)$$

With the variance constraint, the expressions of the gradients in multi-view CCA and PLS are the same as

$$\begin{aligned} \frac{\partial \mathcal{J}}{\partial \mathbf{H}_i} &= \frac{\partial \text{Tr} \left( \sum_{i=1}^V \sum_{\substack{j=1 \\ j \neq i}}^V \mathbf{W}_i^\top \mathbf{H}_i \mathbf{L} \mathbf{H}_j^\top \mathbf{W}_j \right)}{\partial \mathbf{H}_i} \\ &= \sum_{i=1}^V \sum_{\substack{j=1 \\ j \neq i}}^V \mathbf{W}_i \mathbf{W}_j^\top \mathbf{H}_j \mathbf{L}, \end{aligned} \quad (41)$$

and the gradient for multi-view LDA is

$$\begin{aligned} \frac{\partial \mathcal{J}}{\partial \mathbf{H}_i} &= \frac{\partial \text{Tr} \left( \sum_{i=1}^V \sum_{\substack{j=1 \\ j \neq i}}^V \mathbf{W}_i^\top \mathbf{H}_i \mathbf{L}_B^* \mathbf{H}_j^\top \mathbf{W}_j \right)}{\partial \mathbf{H}_i} \\ &= \sum_{i=1}^V \sum_{\substack{j=1 \\ j \neq i}}^V \mathbf{W}_i \mathbf{W}_j^\top \mathbf{H}_j \mathbf{L}_B^*, \end{aligned} \quad (42)$$

Detailed derivation of (41) and (42) can be found in Appendix B.

#### IV. EXPERIMENTS

In this section, we evaluate the multi-view methods on two important multimedia applications: zero-shot recognition on the Animal with Attribute (AwA) dataset, and cross-modal image retrieval on the Wikipedia and Microsoft-COCO datasets.

##### A. Experimental Setup

We conduct the experiments on three popular multimedia datasets. One common property in these datasets is that multi-modal feature representations can be generated. The Animal with Attribute (AwA) dataset consists of 50 animal classes with 30,475 images in total, and 85 class-level attributes. We follow the same setup as in [27] by splitting 40 classes (24,295 images) to train the categorical model while the rest 10 classes with 6,180 images for testing. Sample images from the test set are shown in Fig. 1. Each animal class contains more than one positive attribute, and the attributes are shared across classes which enables zero-shot recognition. The detailed class labels and attributes are provided in [27].

Wikipedia is a cross-modal dataset collected from the “Wikipedia featured articles” [1]. The dataset is organized in 10 categories and consists of 2,866 documents. Each document is a short paragraph with a median text length of 200 words, and is associated with a single image. We follow the train/test split in [1] who use 2,173 training and 693 test pairs of images and documents.

The third dataset we use is the Microsoft COCO 2014 Dataset [40] (abbreviated as COCO in latter paragraphs). We collect the images belonging to at least one fine-grained category, which amounts to 82,081 training images, and 40,137 validation images. More than 5 human-annotated different captions are associated to each image. We follow the same definition in [40] to use 12 super classes as the class labels, and 91 fine-grained categories as the attributes. The class names and attributes are presented in Table II. The classes that the images belong to are highly semantic, and the same image can have multiple class labels. Meanwhile, similar images may belong to several different classes.

We use the following feature representations in the experiments:

- **Image feature by CNN models:** We employ the off-shelf CNN models as stated in [41] and [29] on all image datasets — Visual features are extracted by adopting two powerful pre-trained models. We rescale the size of the images to  $224 \times 224$ , and set the mini-batch size to 50. We use the output from the *fc8* layer after the dropout from *fc7* in VGGNet with 16 weight layers [42] (denoted as *VGG-16* in latter sections) and the *loss3/classifier* layer from GoogleNet [43]. Both models produce 1000-dimension feature vectors.
- **Class label encoding:** Since each image corresponds to one class label on the AwA and Wikipedia dataset, we can describe the image category mapped from the image

TABLE II: The class labels and attributes on the COCO dataset.

Classes
outdoor, food, indoor, appliance, sports, person, animal, vehicle, furniture, accessory, electronic, kitchen
Attributes
person, bicycle, car, motorcycle, airplane, bus, train, truck, boat, traffic, light, fire, hydrant, stop, sign, parking, meter, bench, bird, cat, dog, horse, sheep, cow, elephant, bear, zebra, giraffe, backpack, umbrella, handbag, tie, suitcase, frisbee, skis, snowboard, sports, ball, kite, bat, baseball, glove, skateboard, surfboard, tennis, racket, bottle, wine, glass, cup, fork, knife, spoon, bowl, banana, apple, sandwich, orange, broccoli, carrot, hot dog, pizza, donut, cake, chair, couch, potted, plant, bed, dining, table, toilet, tv, laptop, mouse, remote, keyboard, cell phone, microwave, oven, toaster, sink, refrigerator, book, clock, vase, scissors, teddy, bear, hair, drier, toothbrush

features. Specifically, we firstly train a 100-dimension skip-gram model [44] on the entire English Wikipedia articles composed of 2.9 billion words. Then we can extract a separate set of word vectors from class labels of our datasets. In order to correlate the word and images, we train a ridge regressor with 10-fold cross-validation to map the *VGG-16* image features to each dimension of the word vectors respectively. The regressor outputs are used as the class label features.

- **Attribute encoding:** We also adopt another important modality from visual attributes on the AwA and COCO datasets. Similar to the generation of class label features, we extract *100-dimension* word vectors over attribute tags using the previously trained skip-gram model. On the AwA dataset, we use the  $50 \times 85$  class-attribute matrix in [45], [46] which specifies attribute probabilities of each class, while on the COCO dataset, we develop a 91-bin feature vector as attributes for each image of which 1’s denote the image has the fine-grained tag and 0’s otherwise. Then, we train a ridge regressor between *VGG-16* image feature and the formulated attribute probabilities. The predicted probabilities associated with each image are used as the attribute feature.
- **Sentence encoding:** A vital feature of cross-modal retrieval system is that we make use of textual features directly. We can find a paragraph of text describing each image on the Wikipedia dataset, while on the COCO dataset, a similar paragraph can be developed by concatenating all captions from the observers which are associated to each image. We generated the sentence vectors from the paragraphs by the pre-trained skip-thoughts model [47]. The model was trained over the MovieBook and BookCorpus dataset [48]. On the Wikipedia, we employ the *combined-skip* vector of 4800 dimensions, while due to the large size of COCO dataset, we only use the *uni-skip* vector of 2400 dimensions.

The Experiment protocol and performance metrics are described below:

- **Zero-shot recognition on the AWA dataset:** We follow a similar experiment pipeline as in [49], and the comparative results show the performance of the proposed multi-view embedding methods. We project the multi-view representations to the latent space. Zero-shot recognition is achieved by semi-supervised label propagation on a transductive hypergraph in the latent space. Specifically, the cross-domain knowledge learned from the common semantic space is transferred to the target space of 10 test animal classes via attributes. The prediction of target classes is undertaken on a hypergraph to better integrate different views. We replace the multi-view linear CCA for joint embedding in [49] with the generalized embedding methods. Since the same hypergraph is used, the recognition results indicate the different performance by the multi-view methods in this paper. For the evaluation metric, we use the average classification accuracy which is also employed in [27], [49].

- **Cross-modal retrieval on the Wikipedia and COCO datasets:** We perform two tasks in cross-modal retrieval, i.e. text query for image retrieval and image query for text retrieval. Moreover, a conventional content-based image retrieval system is evaluated in Section IV-C4. We first extract the query features in their own domains. A latent space is jointly learned from the image features, intermediate features and sentence features. Query features are then projected to the latent space by the trained model. The semantic matching from [1] is performed by training a logistic regressor over the embedded features from all of the ground truth samples which maps the projected features of both queries or to-be-retrieved images/texts towards the class labels. The feature vectors generated from the ground truth class labels is essentially the class vectors, whose number of dimension is the number of classes. We use the class probabilities based on the regressor outputs for matching between modalities.

We present the results using 11-point interpolated precision-recall (PR) curves. The Mean Average Precision (MAP) score, which is the average precision at the ranks where recall changes, can be computed based on the Precision Recall curves. The Average Precision (AP) measures the relevance between a query and retrieved items [50], and the MAP score calculates the mean AP by querying all items in the test set.

## B. Parameter Settings

The dimension  $d$  in the latent space is a pre-defined parameter. We will evaluate the effects of different  $d$  values in the following section. In the experiment, we use  $d = 100$  for linear transforms on all dataset. On the Wikipedia and AWA dataset, we choose  $d = 150$  for kernel mappings, and  $d = 200$  for COCO dataset. For computational efficiency on the AWA and COCO dataset, an approximated RBF kernel mapping is adopted for the non-linear mappings. We set  $\sigma$  in the RBF kernel as the average distance between samples from different views/modalities, which is the natural scaling factor for each dataset. In all of the experiments, the original training

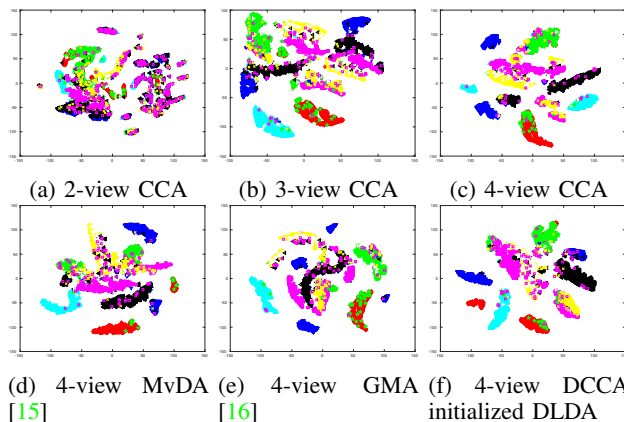


Fig. 4: The first row shows the visualization of a 2-dimensional embedding from the latent space by multi-view linear CCA with increasing number of views on the AWA dataset. The second row presents the embedding maps by different methods all with 4 views on the same dataset. The samples from different classes are denoted in different colors and shapes.

set is further partitioned into a 80% training split and a 20% validation split.

The topology of neural networks has more variabilities, and we chose the optimal one according to the held-out validation set. We refer to [51], [52] for a detailed discussion on topologies. On the AWA dataset, we took 3 hidden layer, each with 1,000 neurons with the *relu* activation before the 100-dimensional linear embedding layer. We only adopted the linear and kernel-based embeddings on the Wikipedia dataset in view of its small size. On the COCO dataset, we chose a single hidden layer with 1500 *relu* neurons, and the dimension of the final linear layer is also 1500. We experimented both with the whole batch and multiple mini-batches for SGD, and adopted a batch size of 200 which achieves a superior performance.

## C. Experimental Results

In the following, we denote LinCCA, LinPLS, SLDA and LinDA as the results by the linear multi-view algorithms, KCCA, KPLS and KDA as the kernel-based methods, KapCCA, KapPLS and KapDA as the methods with the approximated kernel mappings, and DCCA, DPLS and DLDA as the multi-view embedding approaches by (deep) neural networks. SLDA shows the results of the multi-view extension of the standard LDA with (29), and the rest results of the discriminant analysis are obtained using (31).

1) *Results on zero-shot recognition:* We visualize the embedded space in Fig. 4. In the first row, it is shown with the increasing number of views in CCA, the feature vector progresses from being distributed incoherently to showing more distinct groups. In the second row, we compare different methods with 4 views. Instead of a random initialization, we include the result of training a 4-view DLDA initialized by the trained weights from the DCCA networks. It is clearly shown we obtain a set of more compact and separable features from the last method.

Recognition accuracy of different methods is compared quantitatively in Table III. The first group contains the linear



TABLE III: RECOGNITION ACCURACY (%) on the AWA DATASET

Method	2 views	3 views	4 views
LinCCA	56.30	75.06	80.83
LinPLS	59.41	74.52	79.49
SLDA	55.07	72.37	76.34
LinDA	55.73	<b>78.31</b>	81.07
KapCCA	56.41	73.40	74.76
KapPLS	55.58	74.40	75.05
KapDA	57.19	71.64	75.63
DCCA	56.07	74.65	81.43
DPLS	58.69	72.55	75.52
DLDA	53.87	75.41	79.43
DCCA+DLDA	53.55	75.99	<b>81.62</b>
MvDA [15]	<b>60.12</b>	71.03	74.57
GMA [16]	52.12	73.49	78.46
TMV-HLP [49]	-	73.50	80.50
DCCA2 [21]	50.47	-	-

projection results, the second uses the kernel methods, the third are the results by deep neural nets, and the last category includes several comparative results in the literature. Overall, the latent space with linear projections has more discriminative power for this problem, while the non-linear methods are prone to overfitting. The kernel approximation does not provide superior results due to the information loss in sampling. However, the performance of neural network-based approaches improves with more views and increasing size of the training data. Compared to the cold start by DLDA, DCCA initialized 4-view DLDA is reported to be the best method for zero-shot recognition. The results are also organized by the number of views in columns, and it is shown for all methods that we consistently obtain a better accuracy with more views. MvDA [15] achieves the highest accuracy with two input views, while the proposal LinDA has a more discriminant representation in the latent space leading to a better recognition when more views are presented.

2) *Cross-modal retrieval results on the Wikipedia Dataset:* Due to the limited number of samples, we use PCA before performing the subspace learning. We use the VGG-16 features and sentence features for two views, and augment attribute and GoogleNet encodings as the additional modalities. It is shown that a better MAP score is obtained when enriching the latent feature with more modalities as shown in Table IV. We also observe that the supervised methods perform better than the unsupervised counterparts, and non-linear projections by kernel methods are superior. KDA achieves the best retrieval results with supervision and non-linearity.

We present more detailed results in the form of PR curves in Fig. 5. For image queries, KDA consistently outperforms the other methods across all views, which can be explained by its utilization of class labels and kernel-based representations. For text queries, the performance by all methods except LinCCA are comparatively well. The supervised and non-linear methods outperform LinCCA by a large margin. We obtain comparable curves by MvDA [15], SLDA and LinDA, which are the best linear methods in querying text for image retrieval.

3) *Cross-modal retrieval results on the COCO Dataset:*

The COCO dataset is much larger than the Wikipedia dataset, and we pay more attention to the non-linear methods especially the ones using neural networks. Many images have more than one class labels, and therefore we focus on the unsupervised learning algorithms. Similar to the experiments above, the MAP scores in Table V show that a gain of retrieval accuracy can be obtained by embedding additional modalities into the latent space. DCCA2 [21] achieves a better performance with 2 views thanks to its non-linear projection which makes the latent feature more discriminant for retrieval. However, its formulation limits the algorithm to 2 views, and DCCA and DPLS based on the proposed framework can improve the state-of-the-art method by increasing the number of modalities. From the PR curves in Fig. 6, we compare the methods using the proposed objective function with DCCA2 which contains two views. For image queries, KapCCA obtains the best retrieval result with 2 views, but it is further improved by the methods using neural networks benefitted by attributes and GoogleNet features. For text queries, it also suggests more modalities and neural network-based representations contribute to the retrieval performance. The cross-modal retrieval by the 4-view DCCA achieves the overall highest precision score on this dataset.

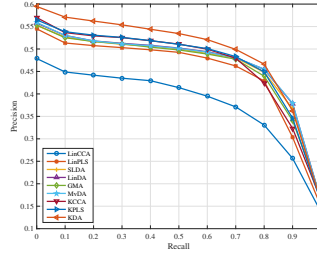
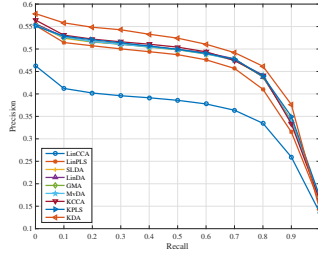
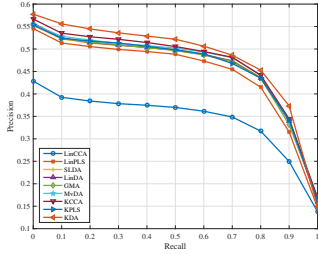
4) *Content-based Image Retrieval (CBIR) Performance on the COCO dataset:* We also show the effectiveness of multi-view embedding method on the conventional CBIR task in Fig. 7. We randomly pick two image-to-text pairs as queries, to perform image-to-image retrieval using both the VGG-16 visual feature and the projected visual feature by the 4-view DCCA. We also perform text-to-image retrieval by querying the corresponding captions of the query image used in CBIR in the last column. We observe the CBIR performance can be further improved by incorporating the semantic information. In Table VI, we present the quantitative results of CBIR by the projected visual features. “RAW” in the Table shows the retrieval results by visual features directly, while the rest are the multi-view embedding results. It is shown that more modalities and non-linear projections yield a discriminant latent visual feature, which improves the retrieval performance.

D. *Parameter sensitivity analysis of dimension  $d$  in linear and kernel cases*

The number of dimension of the feature vectors in the latent space is determined by the top  $d$  eigenvectors in the projection matrix, and it is pre-defined in the former experiments. Therefore, we investigate the effect by the variation of  $d$  shown in Fig. 8 and 9, ranging from  $\{10, 20, 50, 100, 150, 200\}$ . The performance on the Wikipedia dataset is reported with both text queries on images and image queries on texts. The results on different number of views are also recorded. In general, we obtain a better retrieval performance when  $d$  is from 50 to 150. It can be explained by the fact that the most informative eigenvectors are included within the range. Therefore,  $d = 100$  was chosen for the multi-view linear embeddings in the experiments. Moreover, we find KDA is insensitive to the dimension change.

TABLE IV: MAP Scores (%) on the Wikipedia

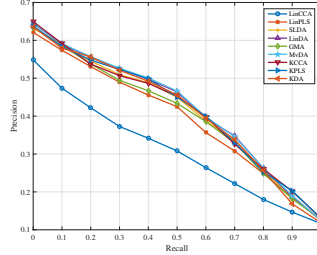
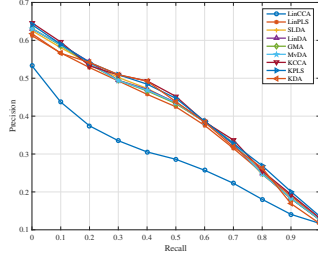
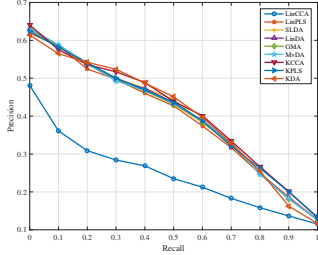
	2 views			3 views			4 views		
	img. query	txt. query	avg.	img. query	txt. query	avg.	img. query	txt. query	avg.
LinCCA	29.93	22.62	26.28	31.99	27.00	29.50	33.55	28.79	31.17
LinPLS	40.51	38.05	39.28	40.76	37.85	39.31	40.72	37.68	39.20
SLDA	42.21	38.83	40.52	42.29	38.76	40.53	42.94	39.31	41.13
LinDA	41.96	38.80	40.38	42.28	38.81	40.55	43.46	39.94	41.70
KCCA	41.02	39.35	40.19	42.57	39.34	40.96	42.63	39.45	41.04
KPLS	42.04	38.95	40.46	42.86	39.36	41.11	43.60	39.73	41.67
KDA	45.26	38.35	<b>41.81</b>	45.66	38.15	<b>41.91</b>	46.20	38.77	<b>42.49</b>
MvDA [15]	42.49	38.78	40.64	42.27	38.77	40.52	43.43	39.16	41.30
GMA [16]	41.91	38.55	40.23	42.26	38.66	40.46	42.26	38.67	40.47



(a) PR curves for image queries with 2 views

(b) PR curves for image queries with 3 views

(c) PR curves for image queries with 4 views



(d) PR curves for text queries with 2 views

(e) PR curves for text queries with 3 views

(f) PR curves for text queries with 4 views

Fig. 5: PR curves across different number of views on the Wikipedia dataset for the Image-to-Text retrieval and the Text-to-Image retrieval.

TABLE V: MAP Scores (%) on the COCO dataset

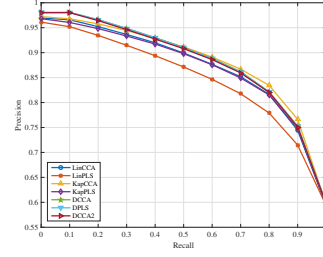
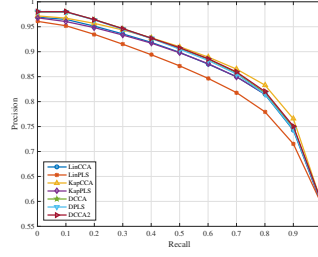
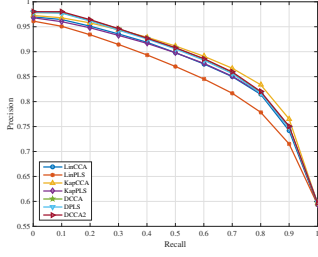
	2 views			3 views			4 views		
	img. query	txt. query	avg.	img. query	txt. query	avg.	img. query	txt. query	avg.
LinCCA	87.18	86.92	87.05	87.20	87.01	87.11	87.31	87.22	87.27
LinPLS	84.76	85.05	84.91	84.83	85.07	84.95	84.82	85.05	84.94
KapCCA	88.42	87.58	88.00	88.35	87.52	87.94	88.45	87.60	88.03
KapPLS	87.16	86.58	86.87	87.14	86.56	86.85	87.14	86.56	86.85
DCCA	88.14	88.10	88.12	88.20	88.26	<b>88.23</b>	88.49	88.40	<b>88.45</b>
DPLS	88.01	88.03	88.02	88.06	88.03	88.05	88.45	88.34	<b>88.40</b>
DCCA2 [21]	88.30	88.27	<b>88.29</b>	-	-	-	-	-	-

TABLE VI: MAP(%) scores of CBIR on the COCO dataset

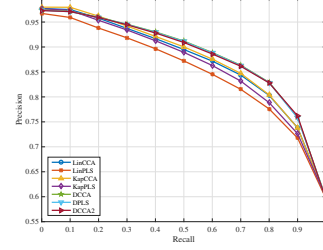
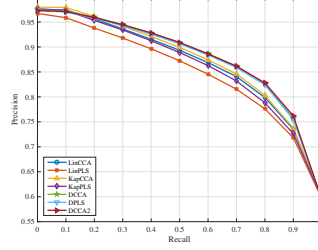
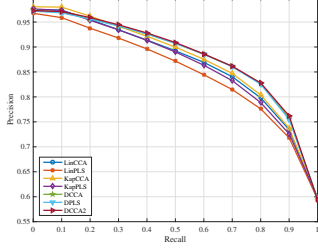
Method	2 views	3 views	4 views
Raw	83.77		
LinCCA	85.64	85.76	85.93
LinPLS	84.30	84.30	84.32
KapCCA	85.43	85.47	85.49
KapPLS	84.56	84.57	84.58
DCCA	89.33	89.62	<b>89.84</b>
DPLS	89.50	89.34	89.79
DCCA2 [21]	89.71	-	-

V. CONCLUSION

In this paper, we proposed a generalized multi-view embedding method using the Rayleigh quotient criterion as the objective function. We showed multi-view CCA, PLS and LDA can be characterized by their specific intrinsic and penalty graph matrices within the same framework. A novel multi-view LDA was introduced by exploiting the distances between class centers of different views. We also studied non-linear embeddings, and found implicit and explicit kernel mappings for multi-view learning. A unified scheme for learning by neural networks was developed which combines the learned representations with a linear embedding layer. We thereby



(a) PR curves for image queries with 2 views (b) PR curves for image queries with 3 views (c) PR curves for image queries with 4 views



(d) PR curves for text queries with 2 views (e) PR curves for text queries with 3 views (f) PR curves for text queries with 4 views

Fig. 6: PR curves across different number of views on the COCO dataset for the Image-to-Text retrieval and the Text-to-Image retrieval. Note the curve by DCCA2 [21] is presented across all numbers of views.

formulated the expression of stochastic gradient descent for optimizing the proposed objective function.

We validated the formulation by conducting experiments in zero-shot visual object recognition and cross-modal image retrieval. It was shown that supervised and non-linear subspace learning outperformed the unsupervised and linear methods when large amount of images and texts were available. Moreover, the recognition or retrieval performance were consistently improved by embedding more views/modalities into the latent feature space. We also performed the traditional CBIR experiments where the multi-view embeddings can contribute their performance gain.

## APPENDIX A

### DERIVATION OF THE BETWEEN-CLASS SCATTER MATRICES $\mathbf{S}_B$ (28) AND $\mathbf{S}'_B$ (30) AND THEIR DIFFERENCE

$$\begin{aligned}
 \mathbf{S}_B &= \sum_{i=1}^V \sum_{j=1}^V \sum_{p=1}^C \sum_{q=1}^C \sum_{p \neq q} (\mathbf{m}_p^i - \mathbf{m}_q^j)(\mathbf{m}_p^i - \mathbf{m}_q^j)^\top \\
 &= \sum_{i=1}^V \sum_{j=1}^V \sum_{p=1}^C \sum_{q=1}^C \sum_{p \neq q} \underbrace{(\mathbf{W}_i \mathbf{X}_i \mathbf{e}_p \mathbf{e}_p^\top \mathbf{X}_i^\top \mathbf{W}_i / N_p^2)}_{\text{term 1}} - \underbrace{\mathbf{W}_j \mathbf{X}_j \mathbf{e}_q \mathbf{e}_p^\top \mathbf{X}_i^\top \mathbf{W}_i / N_p / N_q}_{\text{term 2}} \\
 &\quad - \underbrace{\mathbf{W}_i \mathbf{X}_i \mathbf{e}_p \mathbf{e}_q^\top \mathbf{X}_j^\top \mathbf{W}_j / N_p / N_q}_{\text{term 3}} + \underbrace{(\mathbf{W}_j \mathbf{X}_j \mathbf{e}_q \mathbf{e}_q^\top \mathbf{X}_j^\top \mathbf{W}_j / N_q^2)}_{\text{term 4}}
 \end{aligned} \tag{43}$$

$$\begin{aligned}
 \mathbf{S}'_B &= \sum_{i=1}^V \sum_{j=1}^V \sum_{p=1}^C \sum_{q=1}^C \sum_{p \neq q} (\mathbf{m}_p^i - \mathbf{m}_q^j)(\mathbf{m}_p^j - \mathbf{m}_q^j)^\top \\
 &= \sum_{i=1}^V \sum_{j=1}^V \sum_{p=1}^C \sum_{q=1}^C \sum_{p \neq q} \mathbf{W}_i \mathbf{X}_i (\mathbf{e}_p / N_p - \mathbf{e}_q / N_q) (\mathbf{e}_p / N_p - \mathbf{e}_q / N_q)^\top \mathbf{X}_j^\top \mathbf{W}_j \\
 &= \sum_{i=1}^V \sum_{j=1}^V \sum_{p=1}^C \sum_{q=1}^C \sum_{p \neq q} \underbrace{(\mathbf{W}_i \mathbf{X}_i \mathbf{e}_p \mathbf{e}_p^\top \mathbf{X}_j^\top \mathbf{W}_j / N_p^2)}_{\text{term 5}} - \underbrace{\mathbf{W}_i \mathbf{X}_i \mathbf{e}_q \mathbf{e}_p^\top \mathbf{X}_j^\top \mathbf{W}_j / N_p / N_q}_{\text{term 6}}
 \end{aligned}$$

$$- \underbrace{\mathbf{W}_i \mathbf{X}_i \mathbf{e}_p \mathbf{e}_q^\top \mathbf{X}_j^\top \mathbf{W}_j / N_p / N_q}_{\text{term 7}} + \underbrace{(\mathbf{W}_i \mathbf{X}_i \mathbf{e}_q \mathbf{e}_q^\top \mathbf{X}_j^\top \mathbf{W}_j / N_q^2)}_{\text{term 8}} \tag{44}$$

We compare  $\mathbf{S}_B$  and  $\mathbf{S}'_B$ , and find that term 2, 3, 6, 7 are interchangeable. Term 1 is equivalent to term 4, and term 5 is equivalent to term 8. The difference between the two equations is that term 1 is

$$\begin{aligned}
 \mathbf{S}_{B_1} &= (C-1) \left( \sum_{i=1}^V \sum_{c=1}^C \mathbf{W}_i^\top \mathbf{X}_i \mathbf{e}_c \mathbf{e}_c^\top \mathbf{X}_i^\top \mathbf{W}_i / N_c^2 \right. \\
 &\quad \left. + (V-1) \sum_{i=1}^V \sum_{c=1}^C \mathbf{W}_i^\top \mathbf{X}_i \mathbf{e}_c \mathbf{e}_c^\top \mathbf{X}_i^\top \mathbf{W}_i / N_c^2 \right),
 \end{aligned} \tag{45}$$

while term 5 has

$$\begin{aligned}
 \mathbf{S}'_{B_5} &= (C-1) \left( \sum_{i=1}^V \sum_{c=1}^C \mathbf{W}_i^\top \mathbf{X}_i \mathbf{e}_c \mathbf{e}_c^\top \mathbf{X}_i^\top \mathbf{W}_i / N_c^2 \right. \\
 &\quad \left. + \sum_{i=1}^V \sum_{j=1}^V \sum_{c=1}^C \sum_{j \neq i} \mathbf{W}_i^\top \mathbf{X}_i \mathbf{e}_c \mathbf{e}_c^\top \mathbf{X}_j^\top \mathbf{W}_j / N_c^2 \right)
 \end{aligned} \tag{46}$$

which explains the difference between  $\mathbf{S}_B$  and  $\mathbf{S}'_B$ .

## APPENDIX B

### PROOF OF GRADIENT DERIVATION IN (41) AND (42)

Since we constrain to have a unit variance in the denominator, CCA and PLS then have the same gradient formulation as

$$\frac{\partial \mathcal{J}}{\partial \mathbf{H}_i} = \frac{\partial \text{Tr} \left( \sum_{i=1}^V \sum_{j \neq i}^V \mathbf{W}_i^\top \mathbf{H}_i \mathbf{L} \mathbf{H}_j^\top \mathbf{W}_j \right)}{\partial \mathbf{H}_i} = \sum_{i=1}^V \sum_{j \neq i}^V \mathbf{W}_i \mathbf{W}_j^\top \mathbf{H}_j \mathbf{L} \tag{47}$$

If we replace the Laplacian matrix  $\mathbf{L}$  in multi-view CCA and PLS with  $\mathbf{L}_B$ , then we get






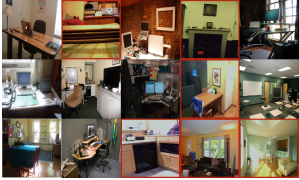

Image Query	Text Query		
	1. A very big building with many windows and a clock on it. 2. A very old tall building with a large clock tower sticking out of it. 3. The clock tower stands high above the city. 4. A clock that is on the side of a large building. 5. The bridge is in front of a huge building with a clock tower in the middle of it.		
Precision: 53.33%	Precision: 86.67%	Precision: 100%	
			
(a) Query by original image feature	(b) Query by projected image feature	(c) Query by text	
Image Query	Text Query		
	1. An open laptop sits on a desk in front of a window. 2. An Apple laptop sitting on a wooden desk. 3. An Apple laptop sitting on a wooden desk in an office. 4. An Apple laptop on a desk in an office. 5. A desk with a laptop sitting on top of it.		
Precision: 60.00%	Precision: 86.67%	Precision: 66.67%	
			
(a) Query by original image feature	(b) Query by projected image feature	(c) Query by text	

Fig. 7: Sample retrieval results on the COCO dataset. The first row of each table presents the query image and text, and the second row shows the retrieved images by different query types. False positive results are bounded in red.

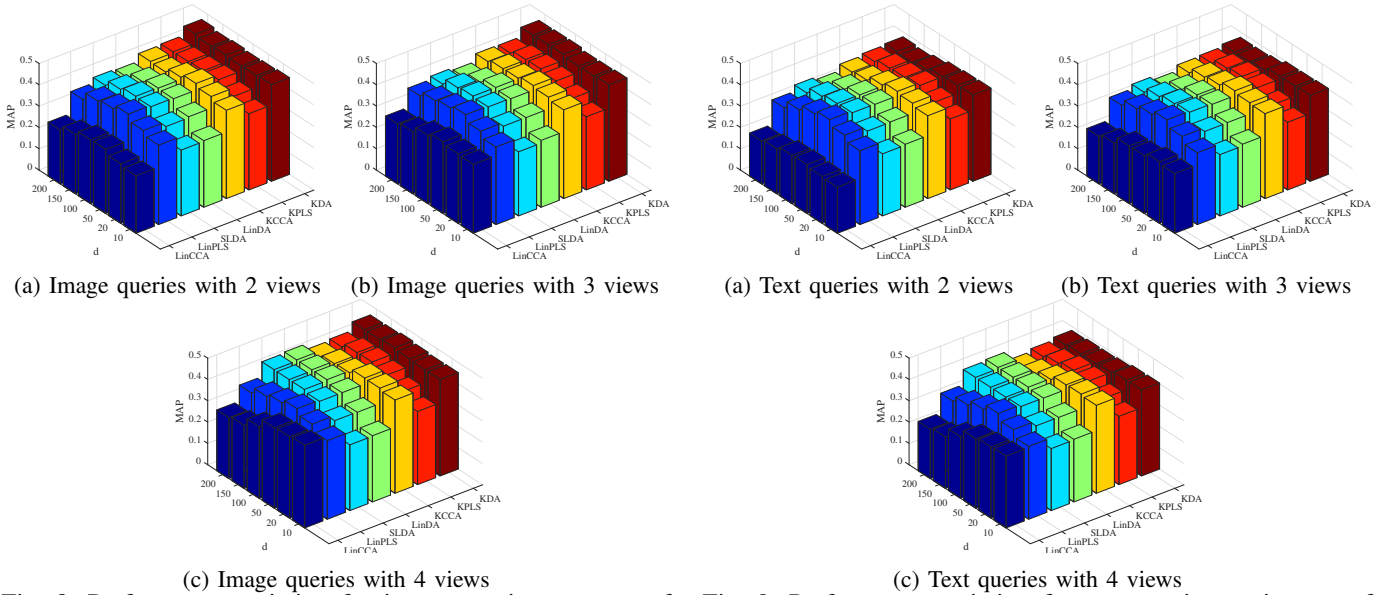


Fig. 8: Performance variation for image queries on texts of Wikipedia dataset with respect to the different dimension  $d$ .

Fig. 9: Performance variation for text queries on images of Wikipedia dataset with respect to the different dimension  $d$ .

$$\frac{\partial \mathcal{J}}{\partial \mathbf{H}_i} = \sum_{i=1}^V \sum_{\substack{j=1 \\ j \neq i}}^V \mathbf{W}_i \mathbf{W}_j^\top \mathbf{H}_j \mathbf{L}_B^*. \quad (48)$$

## REFERENCES

[1] J. Costa Pereira, E. Coviello, G. Doyle, N. Rasiwasia, G. R. Lanckriet, R. Levy, and N. Vasconcelos, "On the role of correlation and abstraction in cross-modal multimedia retrieval," *IEEE Transactions on Pattern*

*Analysis and Machine Intelligence (T-PAMI)*, vol. 36, no. 3, pp. 521–535, 2014.

[2] S. Sun, "A survey of multi-view machine learning," *Neural Computing and Applications*, vol. 23, no. 7-8, pp. 2031–2038, 2013.

[3] K. V. Mardia, J. T. Kent, and J. M. Bibby, *Multivariate analysis*. Academic press, 1980, ch. 10 Canonical Correlation Analysis, pp. 281–290.

[4] A. A. Nielsen, "Multiset canonical correlations analysis and multispectral, truly multitemporal remote sensing data," *IEEE Transactions on Image Processing (TIP)*, vol. 11, no. 3, pp. 293–305, 2002.

[5] Y. Gong, Q. Ke, M. Isard, and S. Lazebnik, "A multi-view embedding

- space for modeling internet images, tags, and their semantics,” *International Journal of Computer Vision*, vol. 106, no. 2, pp. 210–233, 2014.
- [6] H. Hotelling, “Relations between two sets of variates,” *Biometrika*, pp. 321–377, 1936.
  - [7] S. Wold, A. Ruhe, H. Wold, and W. Dunn, III, “The collinearity problem in linear regression. the partial least squares (PLS) approach to generalized inverses,” *SIAM Journal on Scientific and Statistical Computing*, vol. 5, no. 3, pp. 735–743, 1984.
  - [8] T. Diethe, D. R. Hardoon, and J. Shawe-Taylor, “Multiview fisher discriminant analysis,” in *NIPS workshop on learning from multiple sources*, 2008.
  - [9] Q. Chen and S. Sun, “Hierarchical multi-view fisher discriminant analysis,” in *Neural Information Processing*. Springer, 2009, pp. 289–298.
  - [10] S. Yan, D. Xu, B. Zhang, H.-J. Zhang, Q. Yang, and S. Lin, “Graph embedding and extensions: a general framework for dimensionality reduction,” *IEEE Transactions on Pattern Analysis and Machine Intelligence (T-PAMI)*, vol. 29, no. 1, pp. 40–51, 2007.
  - [11] T. Sun, S. Chen, J. Yang, and P. Shi, “A novel method of combined feature extraction for recognition,” in *In Proceedings of IEEE International Conference on Data Mining, (ICDM)*. IEEE, 2008, pp. 1043–1048.
  - [12] Y. Ma, S. Lao, E. Takikawa, and M. Kawade, “Discriminant analysis in correlation similarity measure space,” in *Proceedings of the 24th international conference on Machine learning (ICML)*. ACM, 2007, pp. 577–584.
  - [13] S. Sun, X. Xie, and M. Yang, “Multiview uncorrelated discriminant analysis,” *IEEE Transactions on Cybernetics*, vol. PP, no. 99, pp. 1–13, 2015.
  - [14] Z. Lei and S. Z. Li, “Coupled spectral regression for matching heterogeneous faces,” in *Proceedings of IEEE Conference on Computer Vision and Pattern Recognition (CVPR)*. IEEE, 2009, pp. 1123–1128.
  - [15] M. Kan, S. Shan, H. Zhang, S. Lao, and X. Chen, “Multi-view discriminant analysis,” *IEEE Transactions on Pattern Analysis and Machine Intelligence (T-PAMI)*, vol. 38, no. 1, pp. 188–194, Jan 2016.
  - [16] A. Sharma, A. Kumar, H. Daume III, and D. W. Jacobs, “Generalized multiview analysis: A discriminative latent space,” in *Proceedings of IEEE Conference on Computer Vision and Pattern Recognition (CVPR)*. IEEE, 2012, pp. 2160–2167.
  - [17] J. Liu, Y. Jiang, Z. Li, Z. H. Zhou, and H. Lu, “Partially shared latent factor learning with multiview data,” *IEEE Transactions on Neural Networks and Learning Systems*, vol. 26, no. 6, pp. 1233–1246, June 2015.
  - [18] B. Schölkopf, S. Mika, C. J. Burges, P. Knirsch, K.-R. Müller, G. Rätsch, and A. J. Smola, “Input space versus feature space in kernel-based methods,” *IEEE Transactions on Neural Networks*, vol. 10, no. 5, pp. 1000–1017, 1999.
  - [19] D. R. Hardoon, S. Szedmak, and J. Shawe-Taylor, “Canonical correlation analysis: An overview with application to learning methods,” *Neural computation*, vol. 16, no. 12, pp. 2639–2664, 2004.
  - [20] T. Sun, S. Chen, Z. Jin, and J. Yang, “Kernelized discriminative canonical correlation analysis,” in *International Conference on Wavelet Analysis and Pattern Recognition*, vol. 3. IEEE, 2007, pp. 1283–1287.
  - [21] G. Andrew, R. Arora, J. Bilmes, and K. Livescu, “Deep canonical correlation analysis,” in *Proceedings of the 30th International Conference on Machine Learning*, 2013, pp. 1247–1255.
  - [22] M. Dorfer, R. Kelz, and G. Widmer, “Deep linear discriminant analysis,” *International Conference on Learning Representations (ICLR)*, 2016.
  - [23] T.-H. Chan, K. Jia, S. Gao, J. Lu, Z. Zeng, and Y. Ma, “Pcanet: A simple deep learning baseline for image classification?” *IEEE Transactions on Image Processing (TIP)*, vol. 24, no. 12, pp. 5017–5032, Dec 2015.
  - [24] A. Rahimi and B. Recht, “Random features for large-scale kernel machines,” in *Advances in neural information processing systems*, 2007, pp. 1177–1184.
  - [25] A. Farhadi, I. Endres, D. Hoiem, and D. Forsyth, “Describing objects by their attributes,” in *Proceedings of IEEE Conference on Computer Vision and Pattern Recognition (CVPR)*. IEEE, 2009, pp. 1778–1785.
  - [26] C. H. Lampert, H. Nickisch, and S. Harmeling, “Learning to detect unseen object classes by between-class attribute transfer,” in *Proceedings of IEEE Conference on Computer Vision and Pattern Recognition (CVPR)*. IEEE, 2009, pp. 951–958.
  - [27] —, “Attribute-based classification for zero-shot visual object categorization,” *IEEE Transactions on Pattern Analysis and Machine Intelligence (T-PAMI)*, vol. 36, no. 3, pp. 453–465, 2014.
  - [28] C. Kang, S. Xiang, S. Liao, C. Xu, and C. Pan, “Learning consistent feature representation for cross-modal multimedia retrieval,” *IEEE Transactions on Multimedia*, vol. 17, no. 3, pp. 370–381, March 2015.
  - [29] Y. Wei, Y. Zhao, C. Lu, S. Wei, L. Liu, Z. Zhu, and S. Yan, “Cross-modal retrieval with cnn visual features: A new baseline,” *IEEE Transactions on Cybernetics*, vol. PP, no. 99, pp. 1–12, 2016.
  - [30] R. He, M. Zhang, L. Wang, Y. Ji, and Q. Yin, “Cross-modal subspace learning via pairwise constraints,” *IEEE Transactions on Image Processing*, vol. 24, no. 12, pp. 5543–5556, Dec 2015.
  - [31] L. Van der Maaten and G. Hinton, “Visualizing data using t-sne,” *Journal of Machine Learning Research*, vol. 9, no. 2579–2605, p. 85, 2008.
  - [32] T. Hastie, R. Tibshirani, and J. Friedman, *The Elements of Statistical Learning*. Springer, 2013, ch. 18. High-Dimensional Problems:  $p \gg N$ , pp. 649–694.
  - [33] K. R. Muller, S. Mika, G. Ratsch, K. Tsuda, and B. Scholkopf, “An introduction to kernel-based learning algorithms,” *IEEE Transactions on Neural Networks*, vol. 12, no. 2, pp. 181–201, Mar 2001.
  - [34] B. Schölkopf, R. Herbrich, and A. J. Smola, “A generalized representer theorem,” in *Computational learning theory*. Springer, 2001, pp. 416–426.
  - [35] M. Borge, “Canonical correlation: a tutorial,” <http://people.imt.liu.se/~magnus/cca/tutorial/tutorial.pdf>, 2001.
  - [36] W. Wang, R. Arora, K. Livescu, and J. A. Bilmes, “Unsupervised learning of acoustic features via deep canonical correlation analysis,” in *IEEE International Conference on Acoustics, Speech and Signal Processing (ICASSP)*. IEEE, 2015, pp. 4590–4594.
  - [37] A. M. Martínez and A. C. Kak, “PCA versus LDA,” *IEEE Transactions on Pattern Analysis and Machine Intelligence (T-PAMI)*, vol. 23, no. 2, pp. 228–233, 2001.
  - [38] M. Kan, S. Shan, H. Zhang, S. Lao, and X. Chen, “Multi-view discriminant analysis,” in *Proceedings of European Conference on Computer Vision (ECCV)*. Springer, 2012, pp. 808–821.
  - [39] Y. Jia, F. Nie, and C. Zhang, “Trace ratio problem revisited,” *IEEE Transactions on Neural Networks*, vol. 20, no. 4, pp. 729–735, 2009.
  - [40] T.-Y. Lin, M. Maire, S. Belongie, J. Hays, P. Perona, D. Ramanan, P. Dollár, and C. L. Zitnick, “Microsoft COCO: Common objects in context.” Springer; <http://mscoco.org/home/>, 2014, pp. 740–755. [Online]. Available: <http://mscoco.org/home/>
  - [41] A. Razavian, H. Azizpour, J. Sullivan, and S. Carlsson, “CNN features off-the-shelf: an astounding baseline for recognition,” in *Proceedings of the IEEE Conference on Computer Vision and Pattern Recognition Workshops*, 2014, pp. 806–813.
  - [42] K. Simonyan and A. Zisserman, “Very deep convolutional networks for large-scale image recognition,” *arXiv preprint arXiv:1409.1556*, 2014.
  - [43] C. Szegedy, W. Liu, Y. Jia, P. Sermanet, S. Reed, D. Anguelov, D. Erhan, V. Vanhoucke, and A. Rabinovich, “Going deeper with convolutions,” in *Proceedings of IEEE Conference on Computer Vision and Pattern Recognition (CVPR)*, 2015, pp. 1–9.
  - [44] T. Mikolov, I. Sutskever, K. Chen, G. S. Corrado, and J. Dean, “Distributed representations of words and phrases and their compositionality,” in *Advances in neural information processing systems (NIPS)*, 2013, pp. 3111–3119.
  - [45] C. Kemp, J. B. Tenenbaum, T. L. Griffiths, T. Yamada, and N. Ueda, “Learning systems of concepts with an infinite relational model,” in *AAAI*, vol. 3, 2006, p. 5.
  - [46] D. N. Osherson, J. Stern, O. Wilkie, M. Stob, and E. E. Smith, “Default probability,” *Cognitive Science*, vol. 15, no. 2, pp. 251–269, 1991.
  - [47] R. Kiros, Y. Zhu, R. R. Salakhutdinov, R. Zemel, R. Urtasun, A. Torralba, and S. Fidler, “Skip-thought vectors,” in *Advances in Neural Information Processing Systems*, 2015, pp. 3276–3284.
  - [48] Y. Zhu, R. Kiros, R. Zemel, R. Salakhutdinov, R. Urtasun, A. Torralba, and S. Fidler, “Aligning books and movies: Towards story-like visual explanations by watching movies and reading books,” *arXiv preprint arXiv:1506.06724*, 2015.
  - [49] Y. Fu, T. Hospedales, T. Xiang, and S. Gong, “Transductive multi-view zero-shot learning,” *IEEE Transactions on Pattern Analysis and Machine Intelligence (T-PAMI)*, vol. 37, no. 11, pp. 2332–2345, Nov 2015.
  - [50] C. D. Manning, P. Raghavan, H. Schütze et al., *Introduction to Information Retrieval*. Cambridge university press Cambridge, 2008, vol. 1, no. 1, ch. 8. Evaluation in information retrieval, pp. 188–210.
  - [51] X. Yao, “Evolving artificial neural networks,” *Proceedings of the IEEE*, vol. 87, no. 9, pp. 1423–1447, 1999.
  - [52] S. Kiranyaz, T. Ince, A. Yildirim, and M. Gabbouj, “Evolutionary artificial neural networks by multi-dimensional particle swarm optimization,” *Neural Networks*, vol. 22, no. 10, pp. 1448 – 1462, 2009. [Online]. Available: <http://www.sciencedirect.com/science/article/B6T08-4WGF117-1/2/600b51dc41c51f5fc4c9427b352c7e6a>